Journal of Materials Chemistry A

ROYAL SOCIETY OF CHEMISTRY

PAPER

View Article Online
View Journal | View Issue

Cite this: J. Mater. Chem. A, 2024, 12, 795

Moisture-triggered proton conductivity switching in metal–organic frameworks: role of coordinating solvents†

Hong Kyu Lee,‡[a] Yasaswini Oruganti,‡[b] Jonghyeon Lee,‡[c] Seunghee Han,[d] Jihan Kim,[d] Dohyun Moon, *[e] Min Kim, *[c] Dae-Woon Lim *[b] and Hoi Ri Moon *[f]

Metal–organic frameworks are a good platform for investigating the correlation of structures with physical properties due to the facile coordination environment changes and their responsive structures to external stimuli such as pressure, temperature, and gas sorption. In this study, we report a proton conductivity switching behavior in Zn_5FDC, $[Zn_5(\mu_3\text{-}OH)_2(FDC)_4(solvent)_2]$ (FDC = 9*H*-fluorene-2,7-dicarboxylate) triggered by relative humidity (RH). Interestingly, depending on the presence and absence of coordinating molecules the MOFs show distinctively different tendencies in their proton conductivity. Two isostructural Zn_5FDC compounds, $[Zn_5(\mu_3\text{-}OH)_2(DEF)_2(FDC)_4]$ (Zn_5FDC-DEF) and $[Zn_5(\mu_3\text{-}OH)_2(FDC)_4]$ (Zn_5FDC-OMS; OMS = open metal site), are prepared, in which the three-dimensional connectivities are identical, but the local structures in the secondary building units (SBUs) are different. In the measurement of humidity-dependent conductivity, both MOFs show a dramatic proton conductivity switching phenomenon (ON/OFF ratio, approximately 10^8), but the conductivity switching occurs at different RHs for each MOF (above RH 70% in Zn_5FDC-DEF, and above RH 90% in Zn_5FDC-OMS at 298 K). During this process water coordination in metal centers leads to their structural transformation into Zn_5FDC-H_2O, which means that the different coordination structures by the absence/presence of coordination solvents provide different water access environments to metal centers. The computational calculation supports that the structural transformation of Zn_5FDC-OMS triggered by moisture exposure occurred under higher relative humidity conditions than simple coordination solvent replacement in Zn_5FDC-DEF. This study proves that the coordination solvents play a role in conductivity variation, and it provides a new design strategy for functional solid-state proton conductors.

Received 11th October 2023
Accepted 27th November 2023

DOI: 10.1039/d3ta06197c

rsc.li/materials-a

Introduction

Proton-conductive materials play a pivotal role in proton exchange membrane fuel cells (PEMFC),[1,2] electrolyzers,[3] and CO_2 converters,[4,5] facilitating the generation of clean and efficient electric energy. These applications offer promising renewable energy solutions to mitigate the environmental pollution caused by the combustion of fossil fuels.[6] In addition to well-established proton-conductive materials such as Nafion[7] and oxides,[8] recent attention has been drawn to metal–organic frameworks (MOFs)[9] due to their remarkable design flexibility, high porosity, and crystalline structure. MOFs are emerging as versatile platforms capable of precisely controlling proton conductivity.[10–12] Various methods have been explored to enhance proton conductivity within MOFs, focusing on the induction of continuous hydrogen bonding networks within the MOF pores.[13] These methods involve the decoration of metal centers[14,15] or ligand struts with hydrophilic functional groups,[16,17] as well as the incorporation of suitable guest molecules[18,19] or ions[20] into the MOF pores. These strategies have resulted in the development of MOFs exhibiting exceptional proton conductivity, exceeding 10^{-3} S cm^{-1}, under diverse temperature and humidity conditions.[21–26]

[a]Department of Chemistry, Ulsan National Institute of Science and Technology (UNIST), Ulsan 44919, Republic of Korea

[b]Department of Chemistry and Medical Chemistry, Yonsei University, Wonju, Gangwondo 26493, Republic of Korea. E-mail: limdaewoon@yonsei.ac.kr

[c]Department of Chemistry, Chungbuk National University, Cheongju, Chungbuk 28644, Republic of Korea. E-mail: minkim@chungbuk.ac.kr

[d]Department of Chemical and Biomolecular Engineering, Korea Advanced Institute of Science and Technology (KAIST), Daejeon 34141, Republic of Korea. E-mail: jihankim@kaist.ac.kr

[e]Beamline Department, Pohang Accelerator Laboratory, Pohang, Gyeongbuk 37673, Republic of Korea. E-mail: dmoon@postech.ac.kr

[f]Department of Chemistry and Nanoscience, Ewha Womans University, Seoul 03760, Republic of Korea. E-mail: hoirimoon@ewha.ac.kr

† Electronic supplementary information (ESI) available. CCDC 2300231–2300234. For ESI and crystallographic data in CIF or other electronic format see DOI: https://doi.org/10.1039/d3ta06197c

‡ These authors contributed equally to this work.

Beyond their role as traditional solid-state proton conductors, MOFs exhibit intriguing proton-conductivity switching behavior in response to external stimuli.[27,28] This makes MOFs more fascinating, with potential applications in sensors,[29,30] memory devices,[31–33] and display technologies.[34] The accumulated knowledge derived from studies on the structural dynamics of MOFs under external stimuli, including electric fields,[31,35] guest molecules,[36] and light,[37–39] holds promise for guiding research towards achieving switchable proton conductivity in MOFs. Over the past decade, research on MOFs that demonstrate proton conductivity switching behavior has been growing. Notably, studies focusing on moisture-induced proton conductivity switching in MOFs have identified water molecules as suitable triggers due to their solid donor–acceptor capabilities and ease of control. Moreover, since practical applications like PEMFCs necessitate structural stability in high humidity environments,[40] the investigation of proton conductivity switching MOFs induced by moisture has evolved from understanding reversible proton transport pathways[41] to employing reversible MOFs capable of enhancing proton conductivity under humid conditions.[27] Among these MOFs, Li and Chen[42] reported a novel self-adaptive MOF, BUT-8(Cr)A, which exhibits proton conductivity switching behavior as water molecules induce structural flexibility. BUT-8(Cr)A, with a high density of sulfonic acid groups on its channel surface, ensures a smooth proton conduction pathway across a wide range of humidity conditions. Due to its structural flexibility, BUT-8(Cr)A demonstrates a self-adaptive proton conductive mechanism. The contracted pores gradually open upon water adsorption, maintaining hydrogen bond networks even at low relative humidity. Notably, a significant shift in proton conductivity, from 4.19×10^{-6} to 7.61×10^{-2} S cm^{-1}, was observed as relative humidity increased from 11% to 100% at 25 °C, showing a high ON/OFF ratio of 10^4. Research on such proton-conductivity switching MOFs is still in its early stages, and understanding the dynamics of proton transfer and the role of triggers remains a significant challenge. Additionally, the design and synthesis of MOFs with excellent stimulus responsiveness, including high conductivity, a high ON/OFF ratio, and stable cycling ability, continue to be areas of active investigation.[27]

Herein, we report moisture-triggered switchable proton conductivity in Zn-based MOFs, $[Zn_5(\mu_3\text{-}OH)_2(FDC)_4]$ (Zn_5FDC, FDC = 9*H*-fluorene-2,7-dicarboxylate), which show a dramatic conductivity change of more than 10^8 S cm^{-1} within a narrow relative humidity range. Interestingly, depending on the presence and absence of coordinating molecules in secondary building units (SBUs) of Zn_5FDC, the conductivity switching occurs in different ranges of relative humidity (RH). X-ray diffraction studies and theoretical calculation results explain these phenomena: during the proton conductivity measurement, Zn_5FDC MOFs with and without coordinating molecules undergo a structural transformation upon water coordination, and the difference in the coordination environment affects the threshold structure transformation triggered by H_2O molecules. This study provides empirical data and theoretical substantiation for understanding the influence of coordinating solvents on the proton conduction behaviour in MOFs, contributing to the design strategy for a new functional proton conductor.

Results and discussion

Synthetic strategies of MOFs with/without coordinating solvents

Zn_5FDC, $[Zn_5(\mu_3\text{-}OH)_2(FDC)_4(solvent)_2]$, is an appropriate structure for studying the relationship between local structures and properties influenced by different coordinating solvents within the same frameworks (Scheme 1). Zn_5FDC is composed of pentanuclear Zn clusters coordinating with two solvent molecules and four FDC^{2-} ligands. The coordinating solvents in Zn_5FDC could be adjusted depending on the synthetic strategy, resulting in Zn_5FDC-DEF, $[Zn_5(\mu_3\text{-}OH)_2(FDC)_4(DEF)_2]$, adopting *N*,*N*-diethylformamide (DEF) as a strong coordinating solvent, and Zn_5FDC-DCM, $[Zn_5(\mu_3\text{-}OH)_2(FDC)_2(DCM)_2]$, utilizing dichloromethane (DCM) as a weak coordinating solvent.

Zn_5FDC-DEF is synthesized *via* a solvothermal reaction using H_2FDC and $Zn(NO_3)_2 \cdot 6H_2O$ dissolved in DEF at 85 °C for 48 h. Single-crystal structure analysis revealed that Zn_5FDC-DEF has the *Pccn* orthorhombic space group, exhibiting pcu net topology composed of $Zn_5(OH)_2(DEF)_2$ clusters as octahedral SBUs and FDC^{2-} ligands (Table S1, S2, and Fig. S1†). In the pentanuclear Zn clusters, center Zn has octahedral coordination geometry with six oxygen atoms, where two of them come from bridging μ_3-OH and the others are carboxylate oxygen of the ligand. Meanwhile outer four Zn atoms have tetrahedral coordination geometry, where two of the Zn metals have one coordinating DEF solvent, one bridging μ_3-OH, and two carboxylate oxygen of the ligand. In the thermogravimetric analysis, Zn_5FDC-DEF is stable until 400 °C, and the coordinate DEF solvents continuously released around 200–400 °C, exhibiting 6% of weight loss (Fig. S2†). This weight loss corresponding to DEF molecules was also observed after conducting a solvent exchange process with DCM, which was also confirmed through nuclear magnetic resonance (NMR) studies after digesting the MOF samples (Fig. S3†). This means that preparing Zn_5FDC with OMSs is challenging through solvent exchange as well as activation of Zn_5FDC-DEF. Therefore, we tried to introduce a weak coordinating solvent into Zn_5FDC through a solvent-induced structural transformation approach.[43,44] By adjusting the temperature and concentration of metal and ligand based on the synthetic condition of Zn_5FDC-DEF, we obtained the other types of MOFs, $(H_3O)_2[Zn_8(\mu_3\text{-}O)_3(FDC)_6]$ (Zn_8FDC) and $[Zn_7(\mu_3\text{-}OH)_3(FDC)_6(H_3O)]$ (Zn_7FDC), as a mixture. The structures of Zn_8FDC and Zn_7FDC analysed by single crystal X-ray diffraction (SCD) are described in the ESI (Table S4–S6 and Fig. S4, S5).† Interestingly, both phases converged into Zn_8FDC *via* the reassembly of the metal cluster after immersion in DEF solvent for three days (Fig. S6†). It exhibits a similar trend to previously reported solvent-mediated interpenetration transitions (Fig. S7†).[45]

Subsequently, Zn_8FDC underwent additional solvent-induced structure transformation into Zn_5FDC-DCM during

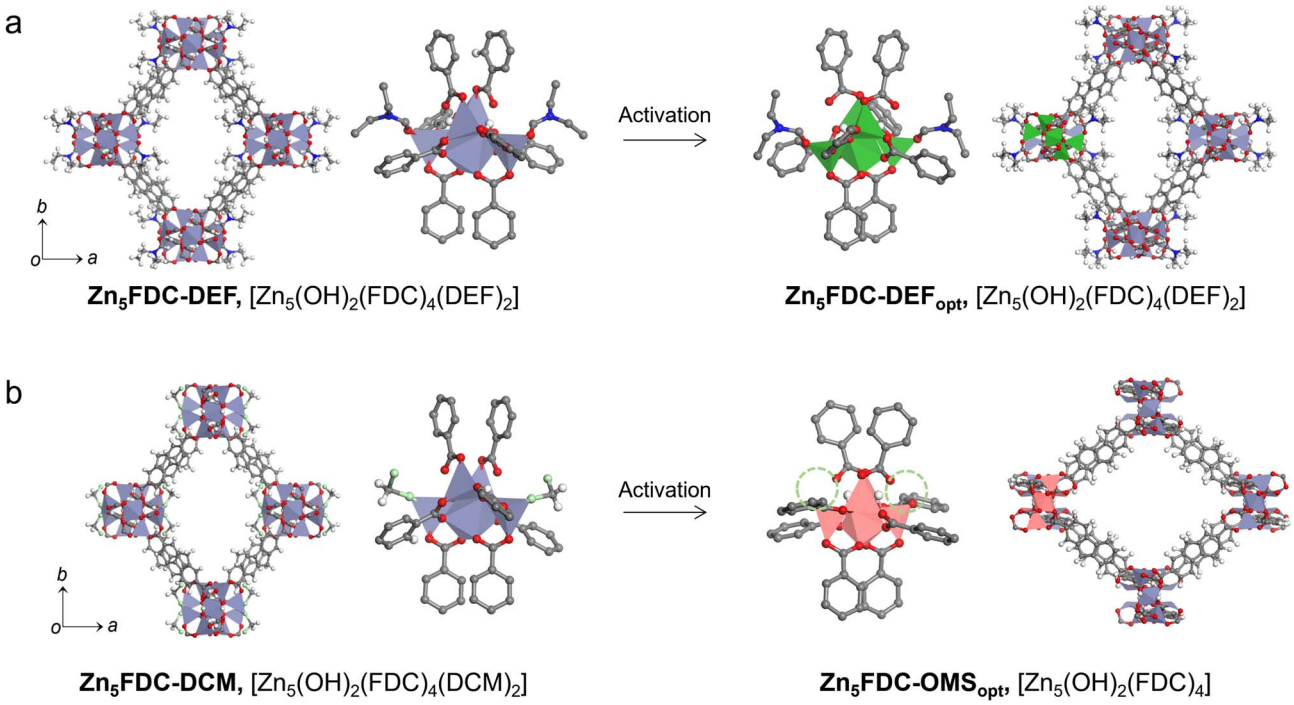

Scheme 1 Structural transformation of (a) Zn_5FDC-DEF and (b) Zn_5FDC-DCM upon activation. The activated structures, Zn_5FDC-DEF_{opt} and Zn_5FDC-OMS_{opt}, were obtained by optimizing the geometry of Zn_5FDC-DEF and Zn_5FDC-DCM after removing coordinating DCM, respectively. Steel blue: Zn, light green: Cl, grey: C, red: O, blue: N, white: H.

the solvent exchange process with DCM, which is isostructural with Zn_5FDC-DEF (Fig. 1, S8 and Table S1, S3†). Both have similar cell parameters except for the *a*-axis due to the size difference of the coordinating solvent. To understand the structure transformation mechanism, we compared the simplified networks based on SCD analysis using the oxo molecules of Zn_8FDC and the hydroxy molecules of Zn_5FDC-DCM as dots and the organic linkers as lines (Fig. S9†). The structural transformation was induced by the loss of metals and ligands and the transition of oxo groups to hydroxy groups in SBUs in DCM. Through this transformation, Zn_5FDC with weak coordinating solvents, namely Zn_5FDC-DCM, was successfully prepared (Fig. 1b).

Water sorption and structural transformation

While Zn_5FDC-DEF retains its coordinating DEF molecules during the DCM exchange and activation processes, Zn_5FDC-DCM readily releases its coordinating DCM molecules, resulting in the formation of Zn_5FDC-OMS during the activation process at 120 °C under vacuum for 16 h. In Fig. 2a, Fourier transform infrared (FT-IR) spectra support these phenomena; in Zn_5FDC-OMS the C–Cl stretch at 730 cm^{-1} disappears, but Zn_5FDC-DEF_{DCM} (Zn_5FDC-DEF soaked in DCM) and Zn_5FDC-DEF_{act} (Zn_5FDC-DEF heated at 120 °C under vacuum) still show $C{=}O_{DEF}$ stretch at 1650 cm^{-1}. To examine the behaviours of Zn_5FDC-DEF and Zn_5FDC-OMS in moisture, the structures of both MOFs were monitored by X-ray powder diffraction (XRPD) after exposure to RH 95% at 25 °C for 48 h. To prevent dew formation and maintain the RH during this experiment, a saturated potassium nitrate solution[46] was used inside a sealed container. As shown in Fig. 2a, upon exposure to moisture, a coordinating water peak appears around 3600 cm^{-1} for both MOFs, Zn_5FDC-H_2O_{DEF} and Zn_5FDC-H_2O_{OMS}, suggesting that water molecules coordinate with the SBUs. Particularly, the replacement of coordinating molecules in Zn_5FDC-DEF is supported by the reduced intensity for the $C{=}O_{DEF}$ stretch at 1650 cm^{-1}. Zn_5FDC-H_2O_{DEF} and Zn_5FDC-H_2O_{OMS} exhibit the same XRPD patterns (Fig. 2b), indicating that Zn_5FDC-DEF and Zn_5FDC-OMS converge into the same structure, Zn_5FDC-H_2O. When compared to the XRPD patterns of the original structures, it can be observed that the coordinating H_2O molecules enable the formation of hydrogen bonds with surrounding oxygen in the metal cluster, inducing overall structure shrinkage. It is worth noting that even after undergoing the activation and subsequent water adsorption processes, the metal–ligand coordination remains intact, as shown in FT-IR spectra; the peaks for $C{-}O_{carboxylate}$ around 1500–1600 cm^{-1} exhibit no alteration.

After activation processes SCD analysis for Zn_5FDC-DEF and Zn_5FDC-DCM failed due to their low crystallinity. In order to predict structural changes during the activation, geometry optimization was performed on Zn_5FDC-DEF and Zn_5FDC-DCM removing coordinating DCM using Materials Studio.[47] The simulated XRPD patterns obtained from optimized structures (denoted as 'opt' in a subscript after their names such as Zn_5FDC-OMS_{opt} and Zn_5FDC-DEF_{opt}) were compared with empirical XRPD patterns (Fig. S10†). The geometry optimization clearly supports that the relatively broader peak of Zn_5FDC-OMS (*e.g.* Zn_5FDC-DCM after activation) than Zn_5FDC-DEF in XRPD patterns is derived from an anisotropic peak shift, where its

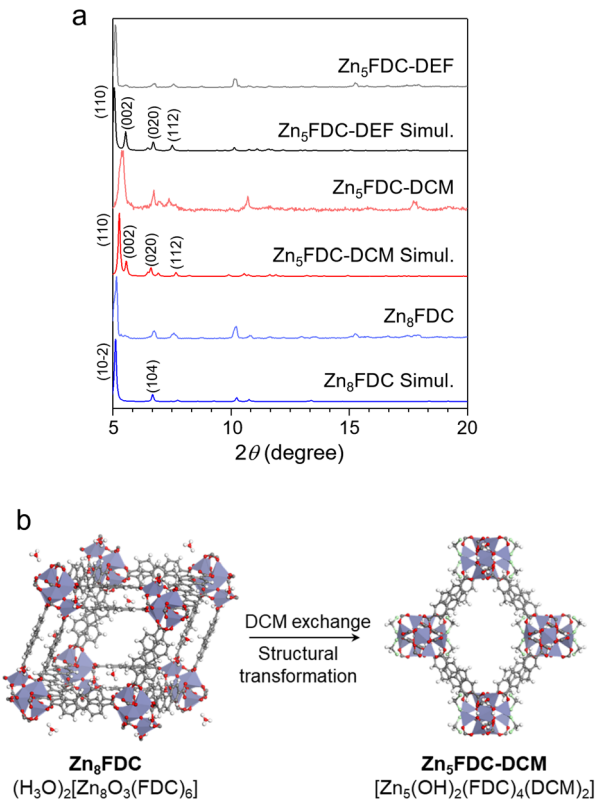

Fig. 1 (a) Comparison of XRPD patterns of Zn_8FDC, Zn_5FDC-DCM, and Zn_5FDC-DEF with their simulated patterns from single crystal structures. (b) Structural transformation of Zn_8FDC into Zn_5FDC-DCM during solvent exchange with DCM. Steel blue: Zn, light green: Cl, grey: C, red: O, white: H.

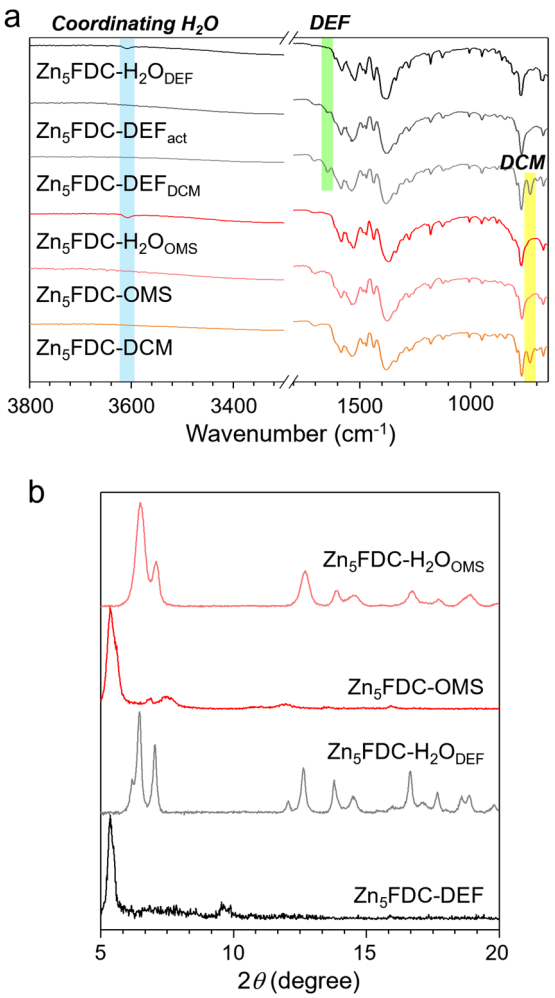

Fig. 2 (a) FT-IR spectra of Zn_5FDC-DCM, Zn_5FDC-OMS, Zn_5FDC-H_2O_{OMS}, Zn_5FDC-DEF_{DCM}, Zn_5FDC-DEF_{act}, and Zn_5FDC-H_2O_{DEF}. (b) The XRPD patterns of activated and water-exposed structures for Zn_5FDC-OMS and Zn_5FDC-DEF.

direction in the same plane for Zn_5FDC-OMS and Zn_5FDC-DEF is opposite. For instance, (110) and (002) planes for Zn_5FDC-OMS shift to lower and higher angles than Zn_5FDC-DCM, respectively, whereas those are opposite in Zn_5FDC-DEF (Fig. S11†). It implies that O–Zn–O bond angles attaching the coordinating solvents to Zn changed depending on the presence of coordinating solvents during the activation process, as a result, the arrangement of the lattice also changed accordingly (Table S7†). Therefore, the distance of the OMS and the hydrogen of benzene and the oxygen of carboxylate in the neighbouring ligand became closer to stabilize the geometry of the OMS in SBUs of Zn_5FDC-OMS (Fig. S12†). In contrast, since coordinating DEF molecules in Zn_5FDC-DEF were bonded to SBUs even after the activation process, only small lattice changes occurred upon bending and rotating of the ligand (Fig. S13†). These local structural differences, with and without coordinating solvent molecules, can lead to a trending preference for H_2O coordination to SBUs, which will play a key role in proton conductivity switching.

Prior to conducting proton conductivity measurements, water vapor sorption experiments were performed on both Zn_5FDC-DEF and Zn_5FDC-OMS. Both MOFs exhibited water uptake at 298 K (Fig. 3), despite being revealed as nonporous materials in N_2 sorption isotherms at 77 K (Fig. S14†). While Zn_5FDC-OMS displayed a linear increase of water uptake as RH increased, Zn_5FDC-DEF exhibited a stepwise uptake isotherm around RH 90%, which might correspond to structural transformation. Additionally, the difference in total uptake amounts between Zn_5FDC-DEF (131 cc g^{-1}) and Zn_5FDC-OMS (168 cc g^{-1}) can be attributed to the presence or absence of coordinating solvents. The desorption profile having a large hysteresis reveals that the adsorbed water was not completely removed from Zn_5FDC-OMS and Zn_5FDC-DEF, implying that water molecules strongly bound to the metal center are difficult to remove. The second cycle of water sorption conducted after evacuation provides indirect evidence for water coordination through a similar reduction in adsorption capacity (50 cc g^{-1}, 3 mol^{-1}), which is approximately consistent with the remaining water in the first cycle.

Switchable proton conductivity

We examined proton conductivity for Zn_5FDC-DEF and Zn_5FDC-OMS and clarified the effects of moisture adsorption tendencies and coordinating solvents on their proton conductivity. To

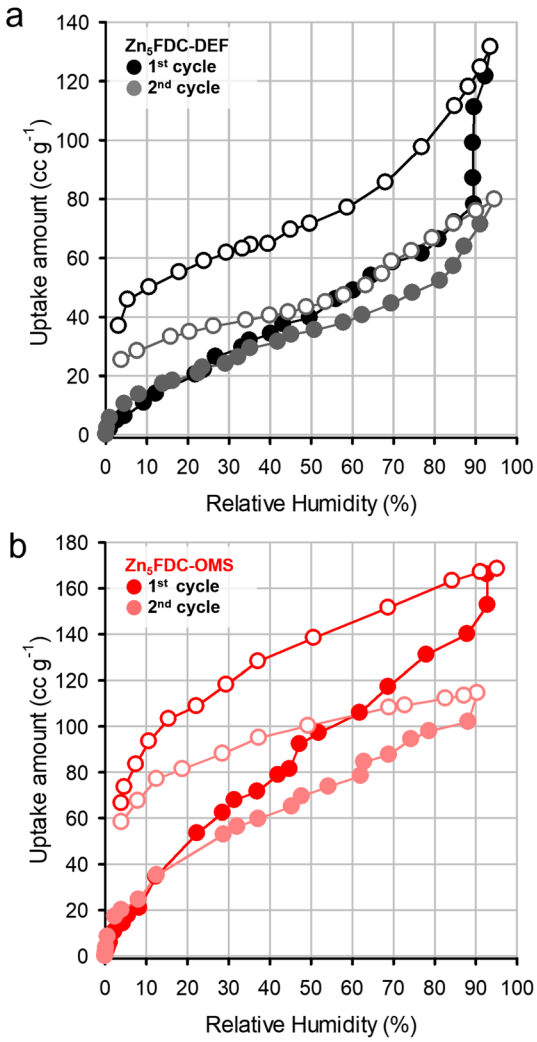

Fig. 3 Water vapor sorption isotherms of (a) Zn_5FDC-DEF and (b) Zn_5FDC-OMS at 298 K.

verify the proton conductivity, the impedance measurements for both MOFs were conducted at different RHs ranging from 30% to 95% and temperatures (Fig. 4a, S15, and Table S9†). At RH 30% and 298 K, the proton conductivities of Zn_5FDC-OMS and Zn_5FDC-DEF are negligible ($<10^{-12}$ S cm^{-1}). Although humidity increased from 30 to 90%, the conductivity of Zn_5FDC-OMS exhibited only a modest one-order increase, indicating the conductivity values of 3.33×10^{-12} S cm^{-1} at 298 K and RH 90%. In contrast, Zn_5FDC-DEF exhibited a continuous improvement of conductivity, and a steep jump occurred above RH 70%, reaching 8.97×10^{-6} S cm^{-1} at RH 90%. This value improved more to 2.49×10^{-4} S cm^{-1} at RH 95%. Zn_5FDC-DEF has the difference between the proton conductivity switching point and steep jump at water sorption because it could exhibit self-adaptive conductivity based on the interaction with water molecules even before its structure is completely transformed by moisture (Fig. S16†). Notably, Zn_5FDC-OMS also exhibits a comparable switching behaviour around RH 90%, showing different conductivity switching points from Zn_5FDC-DEF. Proton conductivity switching can be attributed to the induced structural transformation by pore-filling H_2O as well as coordinating H_2O, which is mainly responsible for proton conductivity due to its acidic properties. Thus, different conductivity switching points in Zn_5FDC-DEF and Zn_5FDC-OMS can be expected to be different interaction energy of H_2O with MOFs at different RH.

In order to understand these phenomena, the interaction energy between water and water as well as water and MOFs at RH 30, 70, and 95% was calculated through RASPA[48] of NVT simulations (Table S8†). This strategy is based on the assumption that proton conductive Zn_5FDC-H_2O would have a strong interaction with moisture from a certain relative pressure after structural transformation compared to the starting materials, and this is known through a comparison of interaction energy according to relative pressure. At RH 30%, Zn_5FDC-OMS exhibits relatively more favourable water–water interaction energy (-17.05 kJ mol^{-1}) and relatively more unfavourable water–MOF interaction energy (-15.36 kJ mol^{-1}) than Zn_5FDC-DEF (-7.319 kJ mol^{-1} and -22.49 kJ mol^{-1}, respectively). It implies that Zn_5FDC-OMS is relatively stable against structure transformation to Zn_5FDC-H_2O induced by moisture exposure compared to Zn_5FDC-DEF at low relative humidity. This tendency is not reversed, even though the energy gap between MOFs is decreased at 70% RH. Thus, the proton conductivity switching behaviour of Zn_5FDC-DEF could occur under lower

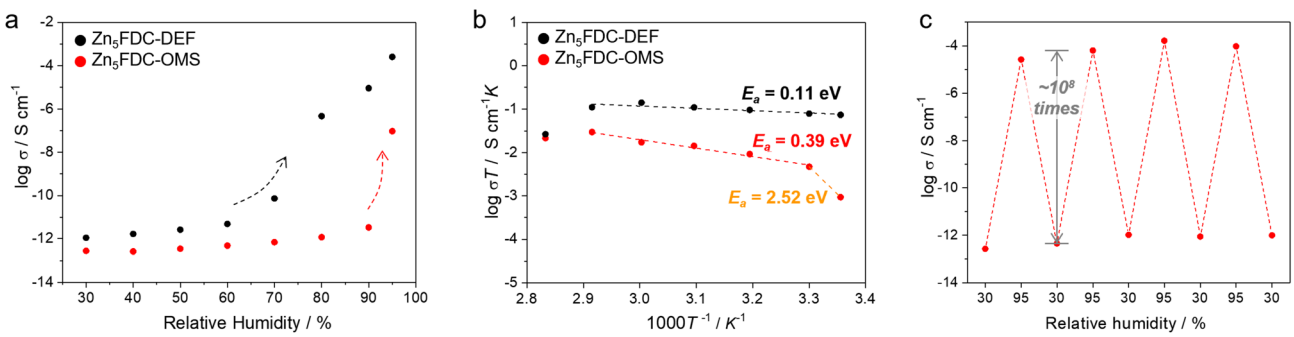

Fig. 4 (a) Proton conductivity of Zn_5FDC-DEF (black) and Zn_5FDC-OMS (red) at 298 K under variable humidity. (b) The activation energy (E_a) from the temperature-dependent conductivity of Zn_5FDC-DEF (black) and Zn_5FDC-OMS (red and orange) measured at RH 95%. (c) Cycling test Zn_5FDC-OMS between 30 and 95% RH at 298 K.

pressure conditions compared to Zn_5FDC-OMS, and DEF to water replacement in Zn_5FDC-DEF could occur under lower pressure conditions than coordination of water in the OMS of Zn_5FDC-OMS. The water–water interaction energy was reversed at 95% RH (water–water interaction energy: Zn_5FDC-OMS; -25.63 kJ mol^{-1}, Zn_5FDC-DEF; -27.13 kJ mol^{-1}), which implies that Zn_5FDC-H_2O_{DEF} has relatively stronger water–water interaction to get a higher conductivity than Zn_5FDC-H_2O_{OMS}.

Subsequently, the temperature-dependent proton conductivity was measured at RH 95%. As illustrated in Fig. 4b, the proton conductivity of both compounds indicates Arrhenius behaviour. The highest proton conductivity value was 8.41×10^{-5} S cm^{-1} for Zn_5FDC-OMS at 80 °C and RH 95% and 4.26×10^{-4} S cm^{-1} for Zn_5FDC-DEF at 60 °C and RH 95% (Table S9†). Further, increased temperature led to a decrease in the conductivity due to the release of guest water molecules. The activation energy (E_a) evaluated from temperature-dependent conductivity for Zn_5FDC-DEF is 0.11 eV, indicating the Grotthuss mechanism of proton conduction where the proton diffuses from one site to another through the hydrogen bond networks. To estimate the activation energy of Zn_5FDC-OMS, the temperature-dependent conductivity plot clearly needs to be divided into two segments. In the range from 298 K to 303 K, the Arrhenius fit of the data results in a relatively high E_a of 2.52 eV, likely associated with the occurrence of a structural transformation.[49] However, the segment from 303 K to 353 K corresponds to the Grotthuss mechanism, featuring a lower E_a of 0.39 eV. This variation in the water-mediated conductivity in the two systems can be ascribed to the potential exchange of coordinated DEF molecules within Zn_5FDC-DEF with guest water occurring even at lower RH at 298 K, resulting in the formation of Zn_5FDC-H_2O_{DEF} and the creation of stable and extensive proton-conducting pathways. Conversely, this exchange is energetically unfavourable in the case of Zn_5FDC-OMS at low RH, as it already possesses a stable geometric configuration. Therefore, it requires relatively higher temperatures where the water molecules are used not only as carriers to transport protons but also to transform the material. The XRPD patterns before and after the water-mediated proton conductivity studies strongly support a structural conversion (Fig. S17†). Finally, both compounds, Zn_5FDC-OMS and Zn_5FDC-DEF, attain the overall same structure (Zn_5FDC-H_2O_{OMS} or Zn_5FDC-H_2O_{DEF}).

In the relative humidity cycling measurement at RH 30% and 95%, these transformed materials exhibit stable conductivity over three cycles, indicating structural stability (Fig. 4c and S17†). Furthermore, Zn_5FDCs demonstrate a superior high on-off ratio of approximately 10^8, compared to other previously reported switchable proton conductive MOFs (Table S10†).

Conclusions

In this study, we reported two isostructural MOFs, Zn_5FDC-DEF and Zn_5FDC-OMS, having different coordinating environments by the presence and absence of coordinating solvents. Both MOFs showed structural transformation upon water uptake under various conditions of relative humidity. The results showed that both MOFs exhibited different response tendencies depending on the relative humidity and temperature, indicating the effects of the presence of coordinating solvents. Specifically, Zn_5FDC-DEF demonstrated a dramatic improvement in conductivity above 70% relative humidity. Meanwhile, Zn_5FDC-OMS showed conductivity at relatively higher humidity levels, RH 90% and maintained its conductivity performance at higher temperatures than Zn_5FDC-DEF.

The difference in the conductive switching points and proton conductivity depending on the temperature of the two MOFs is interpreted to be due to the structural variations of the starting material, influenced by coordinating solvents. Based on temperature-dependent conductivity measurements, both MOFs exhibited Arrhenius behaviours. Notably, Zn_5FDC-DEF has relatively lower activation energy, indicating a Grotthuss mechanism where protons diffuse from one location to another through a hydrogen-bonding network. Finally, cycling experiments verified the structural robustness of these MOFs. Our findings suggest that coordinating solvents play a role in modulating proton conductivity within structurally similar MOFs. This work sets the stage for future investigations into how coordinating solvents impact the proton-conductive properties of MOFs.

Author contributions

H. K. L., Y. O., and J. L. contributed equally to this work. H. K. L. conducted synthesis, characterization, and data analysis. Y. O. conducted water sorption and proton conductivity measurements. J. L. and M. K. performed ligand design and synthesis. S. H. carried out theoretical calculations and analysis. D. M. conducted crystallographic analysis. H. K. L., D.-W. L., and H. R. M. planned the research. All authors contributed to discussions and manuscript writing.

Conflicts of interest

There are no conflicts to declare.

Acknowledgements

This research was supported by the Basic Science Research Program (Grants 2019M3E6A1103980 and 2021R1A2C1003080) through the National Research Foundation of Korea, Korea Basic Science Institute (National Research Facilities and Equipment Center) grant funded by the Ministry of Education (2020R 1A 6C 101B194), and the Regional Innovation Strategy (RIS) grant funded by the Ministry of Education (MOE) (2022RIS-005). X-ray crystallography at the PLS-II 2D SMC beamline of the Pohang Accelerator Laboratory (PAL) is acknowledged.

References

1 A. Kirubakaran, S. Jain and R. K. Nema, *Renewable Sustainable Energy Rev.*, 2009, **13**, 2430–2440.
2 S. M. Haile, *Acta Mater.*, 2003, **51**, 5981–6000.

3 M. Ni, M. K. H. Leung and D. Y. C. Leung, *Int. J. Hydrogen Energy*, 2008, **33**, 2337–2354.
4 R. J. Lim, M. Xie, M. A. Sk, J.-M. Lee, A. Fisher, X. Wang and K. H. Lim, *Catal. Today*, 2014, **233**, 169–180.
5 S. Uhm and Y. D. Kim, *Curr. Appl. Phys.*, 2014, **14**, 672–679.
6 *Fuel Cell Technologies Office Multi-Year Research, Development, and Demonstration Plan*, U.S. Department of Energy, 2016.
7 C. H. Park, C. H. Lee, M. D. Guiver and Y. M. Lee, *Prog. Polym. Sci.*, 2011, **36**, 1443–1498.
8 K. D. Kreuer, *Annu. Rev. Mater. Res.*, 2003, **33**, 333–359.
9 H. C. Zhou, J. R. Long and O. M. Yaghi, *Chem. Rev.*, 2012, **112**, 673–674.
10 D.-W. Lim and H. Kitagawa, *Chem. Rev.*, 2020, **120**, 8416–8467.
11 T. Hou, W. Xu, X. Pei, L. Jiang, O. M. Yaghi and K. A. Persson, *J. Am. Chem. Soc.*, 2022, **144**, 13446–13450.
12 M. Sadakiyo and H. Kitagawa, *Dalton Trans.*, 2021, **50**, 5385–5397.
13 D.-W. Lim and H. Kitagawa, *Chem. Soc. Rev.*, 2021, **50**, 6349–6368.
14 N. C. Jeong, B. Samanta, C. Y. Lee, O. K. Farha and J. T. Hupp, *J. Am. Chem. Soc.*, 2012, **134**, 51–54.
15 S.-S. Liu, Z. Han, J.-S. Yang, S.-Z. Huang, X.-Y. Dong and S.-Q. Zang, *Inorg. Chem.*, 2020, **59**, 396–402.
16 S. M. Elahi, S. Chand, W.-H. Deng, A. Pal and M. C. Das, *Angew. Chem., Int. Ed.*, 2018, **57**, 6662–6666.
17 D. Lee, S. Lee, Y. Son, J. Y. Kim, S. Cha, D. Kwak, J. Lee, J. Kwak, M. Yoon and M. Kim, *Bull. Korean Chem. Soc.*, 2022, **43**, 912–917.
18 W. J. Phang, W. R. Lee, K. Yoo, D. W. Ryu, B. Kim and C. S. Hong, *Angew. Chem., Int. Ed.*, 2014, **53**, 8383–8387.
19 S. Hwang, E. J. Lee, D. Song and N. C. Jeong, *ACS Appl. Mater. Interfaces*, 2018, **10**, 35354–35360.
20 M. Sadakiyo, H. Ōkawa, A. Shigematsu, M. Ohba, T. Yamada and H. Kitagawa, *J. Am. Chem. Soc.*, 2012, **134**, 5472–5475.
21 A. Sharma, J. Lim, S. Jeong, S. Won, J. Seong, S. Lee, Y. S. Kim, S. B. Baek and M. S. Lah, *Angew. Chem., Int. Ed.*, 2021, **60**, 14334–14338.
22 S. C. Pal and M. C. Das, *Adv. Funct. Mater.*, 2021, **31**, 2101584.
23 D. Gui, W. Duan, J. Shu, F. Zhai, N. Wang, X. Wang, J. Xie, H. Li, L. Chen, J. Diwu, Z. Chai and S. Wang, *CCS Chem.*, 2019, **1**, 197–206.
24 Q. Lin, Y. Ye, L. Liu, Z. Yao, Z. Li, L. Wang, C. Liu, Z. Zhang and S. Xiang, *Nano Res.*, 2021, **14**, 387–391.
25 G. K. H. Shimizu, J. M. Taylor and S. Kim, *Science*, 2013, **341**, 354–355.
26 S. Chand, S. M. Elahi, A. Pal and M. C. Das, *Chem. – Eur. J.*, 2019, **25**, 6259–6269.
27 F. Xiang, S. Chen, Z. Yuan, L. Li, Z. Fan, Z. Yao, C. Liu, S. Xiang and Z. Zhang, *JACS Au*, 2022, **2**, 1043–1053.
28 C. Li, K. Wang, J. Li and Q. Zhang, *ACS Mater. Lett.*, 2020, **2**, 779–797.
29 S.-S. Bao, N.-Z. Li, J. M. Taylor, Y. Shen, H. Kitagawa and L.-M. Zheng, *Chem. Mater.*, 2015, **27**, 8116–8125.
30 R. Liu, Y. Liu, S. Yu, C. Yang, Z. Li and G. Li, *ACS Appl. Mater. Interfaces*, 2019, **11**, 1713–1722.
31 Z. Yao, L. Pan, L. Liu, J. Zhang, Q. Lin, Y. Ye, Z. Zhang, S. Xiang and B. Chen, *Sci. Adv.*, 2019, **5**, eaaw4515.
32 Y. Hiruma, K. Yoshikawa and M.-a. Haga, *Faraday Discuss.*, 2019, **213**, 99–113.
33 M.-K. Song, S. D. Namgung, D. Choi, H. Kim, H. Seo, M. Ju, Y. H. Lee, T. Sung, Y.-S. Lee, K. T. Nam and J.-Y. Kwon, *Nat. Commun.*, 2020, **11**, 5896.
34 Y. Wang, R. Shen, S. Wang, Q. Chen, C. Gu, W. Zhang, G. Yang, Q. Chen, Y.-M. Zhang and S. X.-A. Zhang, *Chem*, 2021, **7**, 1308–1320.
35 L. Pan, G. Liu, H. Li, S. Meng, L. Han, J. Shang, B. Chen, A. E. Platero-Prats, W. Lu, X. Zou and R.-W. Li, *J. Am. Chem. Soc.*, 2014, **136**, 17477–17483.
36 R.-L. Liu, W.-T. Qu, B.-H. Dou, Z.-F. Li and G. Li, *Chem.–Asian J.*, 2020, **15**, 182–190.
37 K. Müller, J. Helfferich, F. Zhao, R. Verma, A. B. Kanj, V. Meded, D. Bléger, W. Wenzel and L. Heinke, *Adv. Mater.*, 2018, **30**, 1706551.
38 H.-Q. Liang, Y. Guo, Y. Shi, X. Peng, B. Liang and B. Chen, *Angew. Chem., Int. Ed.*, 2020, **59**, 7732–7737.
39 D.-D. Xu, W.-W. Dong, M.-K. Li, H.-M. Han, J. Zhao, D.-S. Li and Q. Zhang, *Inorg. Chem.*, 2022, **61**, 21107–21114.
40 J. Zhao, Z. Tu and S. H. Chan, *Energy*, 2022, **239**, 122270.
41 M. Sadakiyo, T. Yamada, K. Honda, H. Matsui and H. Kitagawa, *J. Am. Chem. Soc.*, 2014, **136**, 7701–7707.
42 F. Yang, G. Xu, Y. Dou, B. Wang, H. Zhang, H. Wu, W. Zhou, J.-R. Li and B. Chen, *Nat. Energy*, 2017, **2**, 877–883.
43 G. K. Kole and J. J. Vittal, *Chem. Soc. Rev.*, 2013, **42**, 1755–1775.
44 J.-P. Zhang, P.-Q. Liao, H.-L. Zhou, R.-B. Lin and X.-M. Chen, *Chem. Soc. Rev.*, 2014, **43**, 5789–5814.
45 S. B. Choi, H. Furukawa, H. J. Nam, D.-Y. Jung, Y. H. Jhon, A. Walton, D. Book, M. O'Keeffe, O. M. Yaghi and J. Kim, *Angew. Chem., Int. Ed.*, 2012, **51**, 8791–8795.
46 L. Greenspan, *J. Res. NBS. A. Phys. Ch.*, 1977, **81**, 89.
47 BIOVIA. Dassault Systèmes, *Biovia Materials Studio 2017 R2*, Dassault Systèmes, San Diego, 2017.
48 D. Dubbeldam, S. Calero, D. E. Ellis and R. Q. Snurr, *Mol. Simul.*, 2016, **42**, 81–101.
49 R. M. P. Colodrero, P. Olivera-Pastor, E. R. Losilla, D. Hernández-Alonso, M. A. G. Aranda, L. Leon-Reina, J. Rius, K. D. Demadis, B. Moreau, D. Villemin, M. Palomino, F. Rey and A. Cabeza, *Inorg. Chem.*, 2012, **51**, 7689–7698.